2 March 2001

ELSEVIER

Chemical Physics Letters 335 (2001) 381–387

CHEMICAL PHYSICS LETTERS

www.elsevier.nl/locate/cplett

Differential scattering dynamics of $F + CH_4 \rightarrow HF(v,J) + CH_3$ via high-resolution IR laser dopplerimetry

Warren W. Harper, Sergey A. Nizkorodov, David J. Nesbitt *

Department of Chemistry and Biochemistry, University of Colorado and National Institute of Standards and Technology, Boulder, CO 80309-0440, USA

Received 10 October 2000; in final form 8 December 2000

Abstract

Product recoil data from $F + CH_4 \rightarrow HF(v,J) + CH_3$ reactive scattering are obtained using crossed supersonic jets and narrow band ($\Delta\nu \approx 0.0001$ cm^{-1}) infrared radiation laser direct absorption techniques. The high-resolution infrared radiation profiles of $HF(v,J)$ product exhibit extensive Doppler broadening that directly reflects quantum state-resolved *translational* distributions in the laboratory frame under single collision conditions. Analyses of Doppler profiles yield information on state-resolved differential cross sections into the $HF(v=1)$ and $HF(v=2)$ vibrational manifolds, which both identify a propensity for forward/backward scattering ($|\cos(\theta)| \approx 1$) over side scattering ($|\cos(\theta)| \approx 0$) in the center-of-mass frame. © 2001 Published by Elsevier Science B.V.

1. Introduction

State-to-state reactive scattering remains an important focus in chemical physics in efforts to understand simple bond breaking and bond formation dynamics at the most fundamental levels of detail. Recent developments in both theory and experiment are now permitting some of the most rigorous comparisons between quantum state-resolved scattering measurements and numerically converged scattering calculations on ab initio potential energy surfaces. The ability to formulate such high-level comparisons continues to fuel experimental and theoretical advances as well as reveal new physical insights into chemical reaction dynamics. Progress in such state-to-state dynamics has been most notable at the atom + diatom level, with particular emphasis on light atom systems such as $H + H_2$, $F + H_2$, $F + HD$, $O + H_2$, and $Cl + H_2$ [1–6]. Theoretical extension to favorable diatom + diatom systems such as $OH + H_2$ have only recently become accessible in full dimensionality [7]. However, systems with more than one heavy atom, such as the prototypic F atom abstraction reaction from H_2O, NH_3, or CH_4, have remained difficult challenges to address theoretically, due to the many more dynamical degrees of freedom.

In an effort to provide further incentive for the theoretical dynamics community, we have been investigating F atom abstraction reactions based on high-resolution infrared (IR) direct absorption

* Corresponding author. Fax: +1-303-492-5235.
E-mail address: djn@jila.colorado.edu (D.J. Nesbitt).

0009-2614/01/$ - see front matter © 2001 Published by Elsevier Science B.V.
PII: S0009-2614(01)00034-3

methods in crossed supersonic jets [8–12]. In a recent study of $F + CH_4 \rightarrow HF(v,J) + CH_3$ [8], for example, nascent HF product state distributions were determined using direct IR laser absorption under single collision conditions. With $\Delta\nu = 0.0001$ cm^{-1} probe laser resolution, each line also reveals interesting quantum state resolved Doppler structure due to velocity dependent absorption/stimulated emission. This high-resolution structure arises from angular distributions of HF product recoil velocities in the laboratory frame, the careful analysis of which can provide detailed information on state-resolved differential reactive scattering for atom + polyatom systems.

2. Experiment

The experimental details for the crossed jet scattering methods have been reported previously [8] and can be briefly summarized. Two pulsed valves are arranged at right angles; one is a PZT valve [13] used to deliver CH_4 {500 Torr (67 kPa) backing pressure, 145 μm circular orifice, $\leqslant$500 μs pulses}, while the other is an F-atom source consisting of modified solenoid valve {35 Torr (4.7 kPa) backing pressure, 400 μm × 5000 μm slit orifice, ≈2 ms pulses}. The fluorine atoms are produced by electrical discharge at the limiting orifice of the solenoid valve and immediately undergo supersonic expansion. Typical discharge conditions consist of 600 μm spaced electrodes held at −800 V to initiate the discharge, resulting in currents of 250–500 mA. Densities in the jet intersection region are such that the probability of F-atom reaction upon traveling through the CH_4 jet is on the order of 1–2%. This low reaction probability allows us to determine the $HF(v,J)$ initial rates of formation in the absence of secondary collisions that could skew the distribution of recoil velocities. The speeds of the two jets are $v_F = 6.4 \times 10^4$ cm s^{-1} and $v_{CH_4} = 1.15 \times 10^5$ cm s^{-1}, as measured by time-of-flight methods and confirmed by supersonic jet calculations. Angular distributions for each jet have been measured and closely resemble a $\cos^n(\theta)$ distribution that is characterized by a half-width at half-maximum (F source $\theta_{HWHM} = 40°$; CH_4 source $\theta_{HWHM} = 25°$). The jet speeds translate into a perpendicular collision energy of $E_{com} = 1.8(6)$ kcal mol^{-1}, with uncertainty limited by angular distributions for the unskimmed jets.

An amplitude stabilized krypton ion laser (647 nm) is used to pump a color center laser to produce several mW of high-resolution ($\Delta\nu = 0.0001$ cm^{-1}) IR. Most of the IR beam is used for diagnostic purposes (i.e., a scanning Fabry–Perot etalon and traveling Michelson interferometer [14] for relative and absolute frequency calibration, respectively). A small portion (60 μW) of the IR beam is split and used with matched InSb detectors in a dual beam subtraction mode at power levels well below saturation. The HF absorbance is detected as a transient difference signal corresponding precisely to the time profile of the reagent CH_4 gas pulse. This scheme yields an rms absorbance noise of 7×10^{-5} in a 20 kHz detection bandwidth, which is within a factor of 3 of the shot noise limit. Commercially available CH_4 (99.999%) and fluorine mixture (10%:40%:50% F_2:Ne:Ar) are used without further purification.

The high spectral resolution of the probe laser can be further exploited to extract additional dynamical information from the Doppler profiles, which represents the main focus of the present work. Specifically, the F-center laser line width ($\Delta\nu \approx 0.0001$ cm^{-1}) allows products to be characterized with a laboratory frame velocity resolution of ≈10 m s^{-1}, which in principle permits differential cross-section information to be obtained for state-to-state scattering events. The feasibility of such high-resolution IR laser Dopplerimetry methods for obtaining state-resolved differential cross-sections has already been demonstrated, for example, in previous inelastic studies of Cl + HCl [15], rare gas + HF [16], and $Ar + H_2O$ [17] collisions.

Mathematically, the experimentally observed line shapes are expanded in a discrete basis of Doppler profiles generated from Monte-Carlo simulations as a function of center-of-mass scattering angle (θ) and recoil energy (E_{recoil}). Singular value decomposition (SVD) methods [15,16,18–20] are then used to fit the observed Doppler profiles and thereby infer differential scattering cross-sections from the expansion coefficients.

3. Results

High-resolution absorption profiles have been collected for all HF(v,J) product states energetically accessible from the $F + CH_4$ reaction. Doppler profiles are scanned in ~4 MHz increments, yielding ≈1000 points/profile with surrounding baseline. This step size and laser resolution corresponds to a velocity grid of ~8 m s^{-1}, which is 100-fold narrower than the Doppler profiles (0.015–0.030 cm^{-1} FWHM) observed experimentally.

Fig. 1 shows an expanded Doppler profile for the $v = 3 \leftarrow 2$; P(2) HF transition, which exhibits contributions from both *absorption* and *stimulated emission* at large and small Doppler detunings, respectively. Though a more quantitative analysis of this structure will be presented in Section 4, the qualitative physics behind these line profiles is readily identified. At this collision energy (1.8(6) kcal mol^{-1}) and reaction exothermicity [21,22], there is very little excess energy left after formation of HF in the $v = 3$ manifold. Indeed, even in the limit of zero internal excitation in the CH_3 fragment, one still predicts an HF($v = 3, J = 1$) recoil energy of $E_{recoil} \leqslant 1.0$ kcal mol^{-1} appearing as relative translation between the HF and CH_3 fragments. As a result, the stimulated emission contributions arising from population inversion in the HF($v = 3, J = 1$) *upper* state are 'narrow' and concentrated at small Doppler detuning near the line center (depicted in Fig. 1 as a narrow negative profile). Conversely, the HF($v = 2, J = 2$) *lower* state has considerably more energy available ($E_{recoil} \leqslant 11.2$ kcal mol^{-1}) for product translational recoil, which yields a much broader absorption profile spread out over large Doppler detuning (depicted in Fig. 1 as a broad positive profile). The net result of such competing velocity effects is *absorption* in the wings and *stimulated emission* contributions near line center.

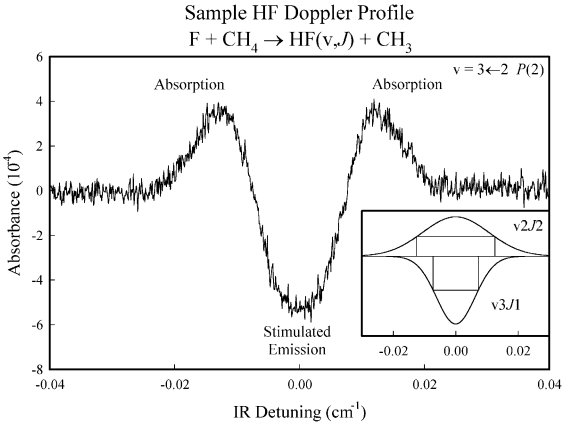

Fig. 1. Doppler profile from a *P*-branch transition in HF illustrating velocity subgroup structure. At small Doppler detuning, the signal exhibits stimulated emission, while at higher detuning the signal is dominated by pure absorption. The inset shows the contributions due to absorption and stimulated emission, drawn with different widths as a consequence of energetic considerations (see text). The shorthand notation $v3J1$ refers to HF($v = 3, J = 1$).

Systematic variations in Doppler line widths are also evident for other transitions, generally *decreasing* with the amount of rovibrational internal energy deposited in HF. For example, the absorption line widths (FWHM) for transitions out of HF(v,J) = (3, 0), (2, 2), and (1, 9) are found to be $\Delta\nu \approx 0.0145(1)$, 0.0229(1), and 0.0277(1) cm^{-1}, respectively. It is worth noting that qualitatively similar velocity dependent structure was also noted previously [9] in HF Doppler profiles from the $F + H_2$ reaction. However, the magnitude of the effect in $F + H_2$ is substantially attenuated by the 20:1 mass difference between HF + H products, which by conservation of momentum and energy, funnels ≈95% of the recoil energy into the unobserved H atom fragment. For the present $F + CH_4$ reaction system, on the other hand, the HF and CH_3 products are nearly equal in mass, which kinematically requires a nearly equal (43%/57% HF/CH_3) sharing of recoil energy. As a result, the high-resolution line profiles carry additional detailed information on laboratory frame velocity distributions for HF(v,J) as a function of rovibrational quantum state. Finally, from previous REMPI studies [23] of CH_3 product state distributions, only a very minor fraction (⩽5%) of the total reaction exothermicity is deposited into the internal modes of the 'spectator' methyl radical fragment. This makes the analysis particularly simple, because for a given exothermicity, collision energy and internal state of the HF(v,J) product, one can therefore obtain the HF and CH_3

transverse recoil velocities and kinetic energy (i.e., along the probe laser) for a specific HF Doppler profile by simple conservation of energy and linear momentum.

4. Analysis

The absorption probe data directly yield nascent HF(v,J) *populations*; to obtain flux necessitates a density to flux transformation, which in turn requires at least partial information on the differential cross-sections. Fortunately, the inferred populations for $F + CH_4$ kinematics and a perpendicular laser detection geometry are not very sensitive to $d\sigma/d\Omega$, which has permitted nascent product state distributions to be readily determined [8]. However, because the individual high-resolution line shapes directly measure the final lab frame velocities along the probe laser axis, such data contain additional information on differential scattering, $d\sigma/d\Omega$, as a function of the center-of-mass angle θ.

The starting point of our Doppler analysis is to generate a discrete basis set in which $(d\sigma/d\Omega)(\cos\theta)$ is to be expanded as a function of scattering angle. For simplicity, this basis set is taken as a set of rectangular step functions of unit height over a finite number of bins distributed uniformly in $\cos(\theta)$. For scattering into a given $\cos(\theta)$ bin at a recoil energy E_{recoil}, the components of v_{HF} *parallel* ($v_{\parallel}$) and *perpendicular* ($v_{\perp}$) to the laser axis can be numerically calculated. Such data is used to increment a histogram representation of the Doppler profile at a given frequency detuning ($v_{\parallel}$), appropriately weighted by residence time ($\propto (1/v_{\perp})$) in the laser beam. These results are integrated over the azimuthal angle ϕ, and repeated for a sufficiently large number (5×10^6) of events for a perpendicular crossed jet collision geometry to generate a smooth representation of the Doppler profile. Most importantly, this procedure correctly incorporates the flux to density transformation, which allows the accumulated Doppler profiles to be reliably predicted for an assumed $d\sigma/d\Omega$ and compared to the experimental results.

The finite angular distribution of the jets can also be included directly in these Monte-Carlo simulations. However, for the present purposes it is much simpler to take these effects into account by convoluting these predictions over Doppler line widths experimentally observed for the energetically highest HF states populated. This should be a reasonable approximation, since the maximum recoil energy corresponds to $<10\%$ of the observed Doppler line widths for HF($v = 3, J = 0$), with even smaller contributions for HF($v = 3, J > 0$). Indeed, in contrast to the HF($v = 0$–2) levels, the experimental Doppler widths in the $v = 4 \leftarrow 3$ manifold are independent of final rotational J state, further confirming that these widths are dominated by angular divergence effects. Examples of the resulting basis functions are presented in Fig. 2 for two values of E_{recoil}, energetically corresponding to products generated in the HF($v = 2, J = 7$) and HF($v = 1, J = 7$) quantum states, respectively. As a consequence of the multipass geometry necessary to enhance detection efficiency, forward versus backward scattering cannot be well characterized, but based on the profiles in Fig. 2, forward/backward ($|\cos(\theta)| \approx 1$) versus sideward ($|\cos(\theta)| \approx 0$) scattering can be clearly distinguished. In principle it is possible to

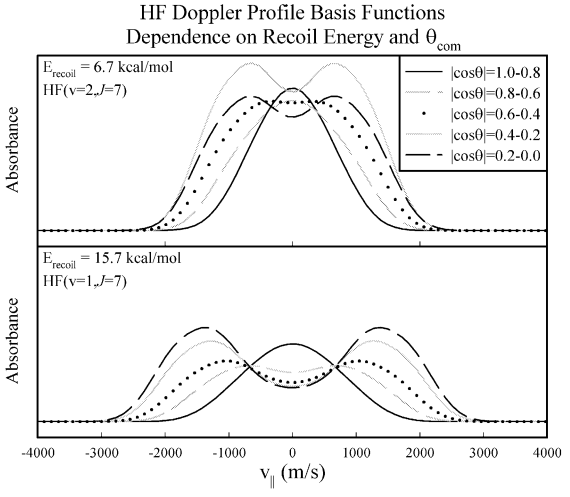

Fig. 2. Sample Monte-Carlo Doppler profiles used as a basis for determining differential cross-sections. These profiles demonstrate experimental sensitivity for distinguishing predominantly forward/backward scattering ($|\cos(\theta)| \approx 1$) versus side scattering ($|\cos(\theta)| \approx 0$) events.

discriminate between forward and backward scattering by using only a single pass of the laser beam with the detection axis in the scattering plane and parallel with the center-of-mass velocity. Unfortunately, the use of a single pass configuration leads to a 20-fold drop in peak intensities, which under our single collision conditions do not produce sufficient signals to determine the differential cross-sections.

The most direct analysis approach would involve simple least-squares fitting of the data with the Monte-Carlo basis functions to determine the differential cross-sections. However, these basis functions are linearly dependent (see Fig. 2) and thus simple least-squares analysis can yield highly correlated results. As demonstrated by previous dopplerimetry studies [15,16,18–20], SVD methods can substantially alleviate these difficulties, in essence by using the Monte-Carlo functions to generate a new linearly independent and orthogonal basis. Only the most significant three of the five orthogonal basis functions need be retained to achieve the level of experimentally observed Doppler structure, which yields a relatively 'coarse grained' representation of $d\sigma/d\Omega$. It is also important to note that the absorption profiles probes population differences and thus depend on both $d\sigma/d\Omega$ in the upper and lower state. However, restricting the analysis to selected transitions dominated by the upper or lower state population can break this additional correlation. By way of example, Fig. 3 presents sample differential cross-section data as a function of $|\cos(\theta)|$ for scattering into several HF(v,J) product states, which clearly indicate a general propensity in the HF($v = 1, 2$) manifold for $|\cos(\theta)| \approx 1$ (i.e., forward–backward) over $\cos(\theta) \approx 0$ (i.e., side scattering). In transitions where differential scattering information can be independently obtained for both upper and lower states, this analysis can be further tested on experimental data with more complicated Doppler structure. For example, Fig. 4 shows representative SVD fits for a series of $HF(v',J') \leftarrow HF(v'',J'')$ transitions, demonstrating that the experimental Doppler profiles can be adequately reproduced for transitions dominated by absorption panel (a), stimulated emission panel (c), as well as transitions exhibiting both absorption and stimulated emission character panel (b).

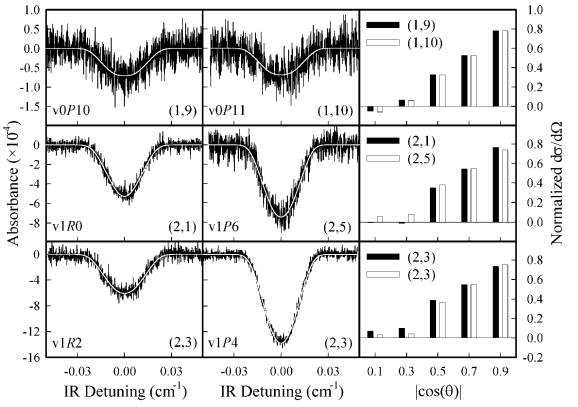

Fig. 3. Differential reactive cross-sections for generating HF(v,J) quantum states in the $v = 1$ and 2 manifolds from SVD methods. The notation in the lower left corner of each panel refers to the lower vibrational/rotational state (e.g., '$v1R2$' implies $v = 2 \leftarrow 1$ and $J = 3 \leftarrow 2$), while the numbers in the lower right corner refers to the v,J state dominating the profiles (upper state in all cases). The differential cross-sections inferred from the SVD analysis indicate a propensity for forward/backward scattering ($|\cos(\theta)| \approx 1$) versus side scattering ($|\cos(\theta)| \approx 0$).

5. Discussion

Although these $F + CH_4$ results are clearly limited in angular resolution, the observed trends are in good qualitative agreement with expectation for fast atom abstraction reactions over a nearly collinear barrier, which lead predominantly to backward scattering of the newly formed product. This is also consistent with the much more detailed differential scattering information available for the energetically similar $F + H_2$ reactive system, which indicate predominantly backward scattering into HF($v \leqslant 2$), with a shift toward more forward scattering in HF($v = 3$). As already noted, additional information on the state-resolved differential scattering trends could be obtained with a unidirectional pass through the scattering region parallel to the relative velocity vector, as well as collimation of the supersonic jets. However, such modifications would require significant loss of

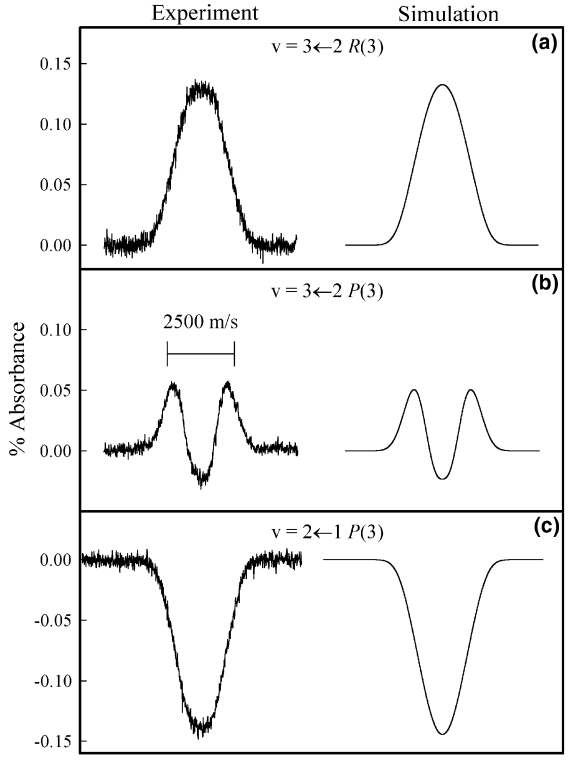

Fig. 4. Simulation (SVD) versus experimental Doppler profiles, demonstrating quantitative fits of panel (a) pure absorption, panel (b) pure stimulated emission, and panel (c) mixed Doppler velocity structure.

absorption path length, which make these studies unfeasible even at near shot noise limited experimental sensitivities.

More quantitatively, the data do reveal a clear relationship between *increasing* Doppler width of the HF profiles and *decreasing* HF internal energy, which can be used to extract additional information on the reactive scattering recoil dynamics. This dynamical correlation is most clearly exhibited in a plot of $\langle E_z \rangle$, the average component of recoil kinetic energy parallel to the probe laser axis, versus E_{HFtot}, the total HF recoil energy. To extract $\langle E_z \rangle$, Doppler profiles for the HF product have been analyzed for a series of J states in the $v = 3, 2, 1$ manifolds, which yields a convolution between the z-axis HF velocity distribution and the experimental response function. Because only average values are required, the distribution in E_z can be approximated as a Gaussian, for which the excess experimental width due to angular jet effects can be removed by subtracting the contributions in quadrature. For such a distribution of molecular velocities, one can readily express the average transverse recoil energy from the standard Doppler formula

$$\langle E_z \rangle = \left(\frac{\Delta \nu_{\mathrm{D}} c}{\nu_0} \right)^2 \frac{M}{16 \ln 2}, \tag{1}$$

where $\Delta \nu_{\mathrm{D}}$ is the deconvoluted Doppler width, ν_0 is the transition frequency, c is the speed of light, and M is the molecular mass. This transverse recoil energy can then be plotted versus the total state-resolved HF(v,J) recoil energy, which can be reliably predicted from reaction exothermicity, center-of-mass collision energy and HF quantum state, neglecting minor (<5%) contributions from the CH_3 internal energy. The resulting correlation plot is depicted in Fig. 5. Limiting cases have been indicated on the figure with dotted lines corresponding to (i) pure side scattering (slope = 1) and (ii) isotropic scattering (slope = 1/3). These data clearly demonstrate a strongly diminished energy release *perpendicular* to the jet intersection plane (i.e., along the laser probe axis), which corre-

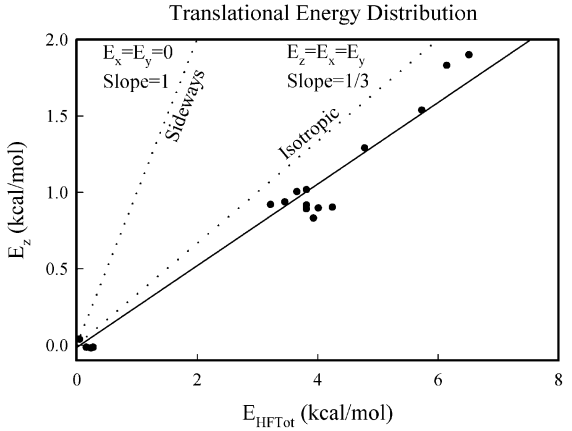

Fig. 5. Recoil energy distribution of HF products. Plotted is the HF recoil energy along the laser axis (E_z) versus the quantum state specific total HF recoil energy (E_{HFtot}) (see text for details). The upper and lower dotted lines represent model predictions for pure sideways versus isotropic scattering; the solid line is a least-squares fit of the data, indicating a small propensity for forward–backward scattering.

sponds to a minimum in the $d\sigma/d\Omega$ differential scattering cross-section for sideways reactive scattering ($|\cos(\theta)| \approx 0$). This is also entirely consistent with trends in $d\sigma/d\Omega$ cross-sections obtained above from the SVD analysis, which indicate a propensity for forward–backward ($|\cos(\theta)| \approx 1$) scattering of product into HF($v = 1, 2$) manifolds.

As a final note, Fig. 5 also unambiguously demonstrates the presence of translationally hot HF product velocities, with transverse HF translational recoil energies as high as $\approx$2 kcal mol^{-1} parallel to the laser detection axis. In light of extremely efficient relaxation of translational degrees of freedom, rovibrational relaxation processes can be expected to contribute negligibly to the product state distributions reported in these crossed jet studies. This is entirely consistent with the collision densities and long mean free path lengths in the jet intersection region. Nevertheless, the absence of translational relaxation provides useful independent confirmation that the reactive scattering dynamics are captured under nascent, single collision conditions.

6. Conclusions

The $F + CH_4 \rightarrow HF(v,J) + CH_3$ reaction has been studied using direct infrared absorption detection in a crossed supersonic jets apparatus. Sub-Doppler resolution (0.0001 cm^{-1}) of the probe laser has revealed Doppler profiles with state specific structure having contributions from absorption and stimulated emission. The Doppler profiles have been analyzed to extract trends in the differential cross-sections as a function of HF vibrational manifold. Line shapes are fit via SVD methods to a basis formed by discrete representation of Doppler profiles as a function of scattering angle $\cos(\theta)$. The fits demonstrate a clear propensity for forward/backward versus side scattering in the HF($v = 1, 2$) manifolds. This result is further underscored by Doppler fits of the average transverse recoil energies along the laser probe axis, which indicate a strong linear correlation with excess reaction exothermicity for a given HF(v, J) quantum state.

Acknowledgements

This research has been funded by the Air Force Office of Scientific Research, with support from the National Science Foundation in the development of the pulsed slit discharge sources. W.H.W thanks the National Research Council for a post-doctoral research fellowship.

References

[1] F.J. Aoiz, L. Banares, V.J. Herrero, J. Chem. Soc., Faraday Trans. 94 (1998) 2483.
[2] K. Stark, H. Werner, J. Chem. Phys. 104 (1996) 6515.
[3] F. Dong, S.H. Lee, K. Liu, J. Chem. Phys. 113 (2000) 3633.
[4] E. Wrede, L. Schnieder, K.H. Welge, F.J. Aoiz, L. Banares, J.F. Castillo, B. Martinez-Haya, V.J. Herrero, J. Chem. Phys. 110 (1999) 9971.
[5] X. Liu, J.J. Lin, S. Harich, G.C. Schatz, X. Yang, Science 289 (2000) 1536.
[6] S.A. Kandel, A.J. Alexander, Z.H. Kim, R.N. Zare, F.J. Aoiz, L. Banares, J.F. Castillo, V.S. Rabanos, J. Chem. Phys. 112 (2000) 670.
[7] D.H. Zhang, S.Y. Lee, J. Chem. Phys. 109 (1998) 2708.
[8] W.W. Harper, S.A. Nizkorodov, D.J. Nesbitt, J. Chem. Phys. 113 (2000) 3670.
[9] W.B. Chapman, B.W. Blackmon, S. Nizkorodov, D.J. Nesbitt, J. Chem. Phys. 109 (1998) 9306.
[10] W.B. Chapman, B.W. Blackmon, D.J. Nesbitt, J. Chem. Phys. 107 (1997) 8193.
[11] S. Nizkorodov, W.W. Harper, W.B. Chapman, B.W. Blackmon, D.J. Nesbitt, J. Chem. Phys. 111 (1999) 8404.
[12] S. Nizkorodov, W.W. Harper, D.J. Nesbitt, Faraday Discuss. 113 (1999) 107.
[13] D. Proch, T. Trickl, Rev. Sci. Instrum. 60 (1989) 713.
[14] J.L. Hall, S.A. Lee, Appl. Phys. Lett. 29 (1976) 367.
[15] Z.Q. Zhao, W.B. Chapman, D.J. Nesbitt, J. Chem. Phys. 104 (1996) 3555.
[16] W.B. Chapman, M.J. Weida, D.J. Nesbitt, J. Chem. Phys. 106 (1996) 2248.
[17] W.B. Chapman, A. Kulcke, B.W. Blackmon, D.J. Nesbitt, J. Chem. Phys. 110 (1999) 8543.
[18] A. Schiffman, W.B. Chapman, D.J. Nesbitt, J. Phys. Chem. 100 (1996) 3402.
[19] H.L. Kim, M.A. Wickramaaratchi, X. Zheng, G.E. Hall, J. Chem. Phys. 101 (1994) 2033.
[20] W.R. Simpson, A.J. Orr-Ewing, R.N. Zare, Chem. Phys. Lett. 212 (1993) 163.
[21] K.-M. Weitzel, M. Malow, G.K. Jarvis, T. Baer, Y. Song, C.Y. Ng, J. Chem. Phys. 111 (1999) 8267.
[22] J.A. Blush, P. Chen, R.T. Wiedmann, M.G. White, J. Chem. Phys. 98 (1993) 3557.
[23] K. Sugawara, F. Ito, T. Nakanaga, H. Takeo, C. Matsumura, J. Chem. Phys. 92 (1990) 5328.